Influence of the Shape Memory Alloys on Concrete Shear Wall with Eccentric Openings

Mohammad Reza Shokoohfar[1], **Mehdi Ghassemieh**[2], **Amin Komeili**[3], **Mohammad Shakerian**[4]

[1] School of Civil Engineering, College of Engineering, University of Tehran; mreza.shokoohfar@ut.ac.ir
[2] School of Civil Engineering, College of Engineering, University of Tehran; m.ghassemieh@ut.ac.ir
[3] School of Civil Engineering, College of Engineering, University of Tehran; amin.komeili.98@ut.ac.ir
[4] School of Civil Engineering, College of Engineering, University of Tehran; mshakerian@ut.ac.ir

Abstract

Seismic loading is crucial in seismically vulnerable nations, and neglecting it can result in catastrophic harm to both structural and non-structural components. Columns, beams, and walls will grow in size and weight due to employing a structure's elastic ability to dissipate seismic energy, which will also raise the cost of construction. Shear walls are frequently employed due to their effective behavior under seismic loads and a strong capacity for energy dissipation. Sometimes, it is unavoidable to prevent openings in shear walls for architectural reasons. Due to load concentration in the vicinity of voids, providing sufficient ductility in these shear walls is challenging. Plastic deformations render the constructions unusable, which is another issue with shear walls. Researchers are paying more and more attention to the use of shape memory alloys (SMA) as reinforcing bars in concrete buildings. This study aims to assess the effectiveness of using superelastic Nitinol (NiTi) and Fe-based (FeMnAlNi) SMAs in a concrete shear wall to reduce residual displacement. One shear wall model without SMA was created with OpenSees finite element software to verify this analysis's integrity. Secondly, the steel rebar was partially replaced with different types of SMA in critical locations. Results indicated that utilization of superelastic alloys would result in a significant reduction of residual displacement. Additionally, a slight change in the shear wall's dissipated energy is observed compared to the shear walls without SMA.

Keywords: Shape memory alloys, Superelastisity, Finite Element Method, Reinforced concrete shear wall, self-centering.

Introduction

Typically, the primary earthquake-resistant elements of reinforced concrete structures are structural walls. However, they often contain a few openings in line with the purpose of the architectural design, and the opening ratios, placements, and forms are frequently different.

However, assessing the stiffness and shear strength of structural walls containing openings is challenging. Evaluation becomes significantly more challenging if the openings are positioned eccentrically. Using a strut and tie model is standard to represent structural walls with eccentric openings. However, the modeling technique is not simple and requires considerable knowledge. Due to variations in design and modeling, both national and international seismic design codes include certain associated structural features and constraints.

In earthquake-prone countries, seismic design plays a significant role. If this factor is not appropriately considered, significant earthquake damage will occur.

Inoue et al. in (1998), Fujita et al. (2001), Palermo and Vecchio (2007), and others have all worked extensively on FEM analyses of structural walls over the recent decades, but the design process always takes much longer [1-3].

The stress concentration in particular places causes compression (crushing) and tensile (cracking) damage in concrete. Proposing ways to prevent or postpone these failures becomes extremely important when they are coupled with significant displacements and unexpected loadings that may negatively influence the shear wall carrying capacity. The persistent damage and deformations of shear walls can be influenced by the type of reinforcement utilized. Ductile materials are required to enhance the shear wall's ability to withstand significant deformations and hold onto modest residual stresses [4].

SMA

The shape-memory effect and superelasticity are two distinctive features of shape-memory alloys (SMAs).

The capacity of the alloys to return to their original shape after heating them to the temperature at which they undergo phase change is known as the shape-memory effect.

SMAs have a particular characteristic that sets them apart from other materials and is directly tied to the atomic structure of the alloy. Austenite, which is stable at high temperature, and Martensite, which is stable at low temperature, are the two distinct atomic structures of SMAs. The heating or stress loading of these phases can cause a reversible transition between them "Figure 1". Superelasticity and the Shape Memory Effect (SME) are two crucial properties of SMAs (SE). Fully Austenite-structured SMAs exhibit SE behavior, whereas Martensite-structured SMAs exhibit SME behavior [5, 6].

Even when it experiences significant inelastic deformations, a superelastic SMA could quickly recover its original shape following unloading. The majority of applications that may use this capability are seismic ones. When heated, SMAs can revert to their predetermined forms because of a feature called SME.

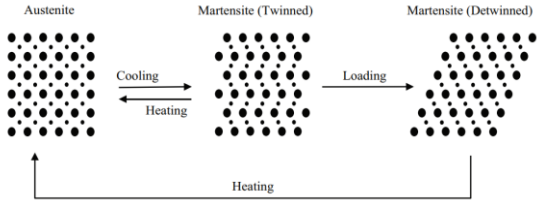

Figure 1. Phase transformation of the SMA [4].

"Figure 2" depicts a superelastic SMA undergoing a loading and unloading cycle in an exemplary stress-strain diagram. The following four stress values are used to define the superelastic model at a constant temperature. There are four types of stress: starting stress from Austenite to Martensite, finishing stress from Austenite to Martensite, starting stress from Martensite to Austenite, and ending stress from Martensite to Austenite [7].

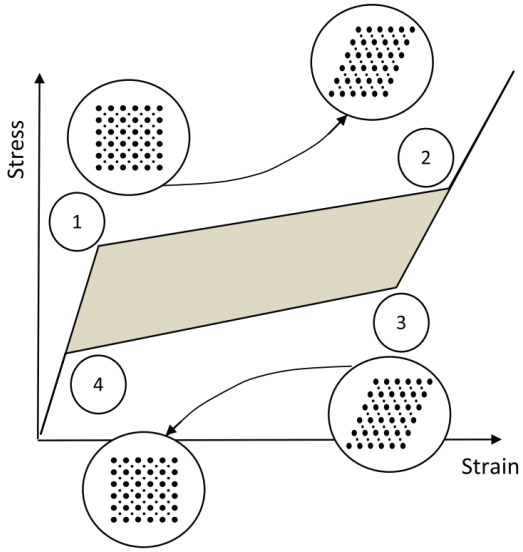

Figure 2. Stress–strain diagram model of 1D-superelastic SMA [4].

There are several advantages and disadvantages associated with various SMAs families. Beginning in the early 1960s, SMAs were created. They have been effectively employed for medical [8, 9], robotic [10], aerospace [11, 12], automotive [13], and Their use in structural and civil engineering is growing.

SMAs could well withstand corrosion, fatigue, and significant deformations.

Dolce and Cardone (2001) subjected superelastic NiTi SMA wires to cyclic tensile testing and concluded that the SMAs' properties are suitable for seismic applications [14]. The utility of SMAs as reinforcement in reinforced concrete (RC) constructions was demonstrated via comprehensive analytical and experimental investigations that followed the advancement of research on these alloys. Czaderski et al. (2006) experimented on an SMA-reinforced RC beam and contrasted it with a standard RC beam. Their findings demonstrated that an RC beam with changeable stiffness and strength might be created utilizing SMAs [15].

The use of SMAs as reinforcement in concrete buildings has been the subject of much research in recent years, but concrete shear walls have not seen the same level of investigation. With the use of a finite element model, Ghassemieh et al. (2012, 2013) assessed the effectiveness of the SMA-reinforced concrete shear walls (without openings) and demonstrated how this reduced the structure's overall permanent residual strain [16, 17]. Additionally, they examined how well SMA reinforcement improved the seismic response of coupled shear walls and concluded that it significantly restored the remaining displacement in the shear wall.

This article examines the impact of shape memory rebars with various SMAs on the concrete shear wall's energy dissipation and residual displacement capacity. To accomplish this, a concrete shear wall with steel bars and eccentric openings is first modeled without SMA, using OpenSees software and an MVLEM macro element, which is explained later. The results of this model are examined to ensure that the results are similar to those in the experimental laboratory results for the purpose of verification. After the verification phase, steel rebars are replaced with various amounts of SMA, and the effects of this change in residual displacement and dissipated energy are analyzed and reported for interpretation.

Model Description

This study adapted one specimen as an analytical object "Figure 3". The experimental tests were carried out at Kyoto University, Japan, and used 40 percent scale models of concrete structural walls with eccentric openings [18,19].

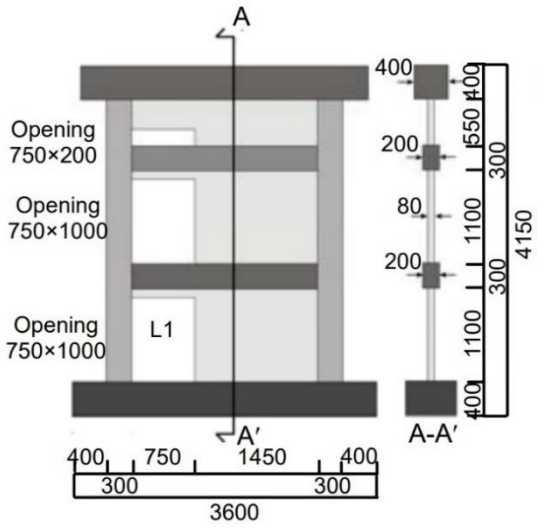

Figure 3. Dimension of specimens (mm)[19]

"Figure 3" illustrates the specimen's height and span length. "Tables 1" and "Table 2", respectively, include a list of the sectional measurements as well as certain specifics about beams, columns, and walls. The various sorts of reinforcements are represented by D and Φ. Table 3 details the material characteristics of the reinforcement used for this sample. The compressive strength (MPa), tensile strength (MPa), and young's modulus (GPa) of the concrete are 28.9, 2.2, and 26.0, respectively. The opening ratio used as an experimental parameter is 0.46 for, defined as $(h_0 l_0/hl)^{1/2}$, where l_0 and h_0 are the length and height of the aperture. The l and h are the center-to-center distances between the upper and lower beams [19].

Table 1. Section and reinforcements of beam/column (mm) [19]

	Section dimension	Main reinforcement	Hoop reinforcement
Side column	300×300	8-D19	2-Φ10@75
Beam	200×300	2-D13	2-Φ6@100
Foundation beam	600×400	4-D25	4-D10@100
Loading beam	400×400	2-D25	2-D10@100

Table 2. Section and reinforcements of the wall (mm) [19]

Thickness (mm)	80
Wall reinforcement	D6@100
Reinforcing bar of opening (vertical)	1-D16
Reinforcing bar of opening (horizontal)	2-D13

Table 3. Properties of reinforcements (mm) [19]

rebar	Yield strength (MPa)	Ultimate strength (MPa)	Young modulus (GPa)
D6	425	538	204
D10	366	509	180
D13	369	522	189
D16	400	569	194
D19	384	616	183
Φ6	985	1143	197
Φ10	962	1085	195

Loading description

After modeling the shear wall, it is recommended to apply the loading depicted in "Figure 4" to the wall that was applied in the experiment and then compare the model's findings with those obtained for validation [19].

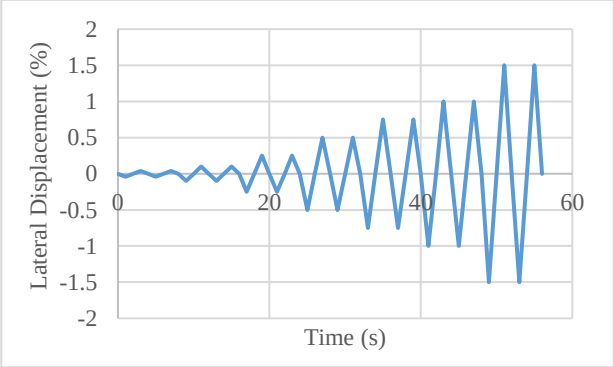

Figure 4. Horizontal loading assigned to shear wall

This loading has fourteen cycles, each of which is performed twice. The relative displacement values for the cycles are ± 0.04 %, ± 0.1 %, ± 0.25 %, ± 0.5 %, ± 0.75%, ± 1.0%, ± 1.5% respectively The model mentioned above could have an excellent relationship with the laboratory results, as seen in "Figure 5" [19].

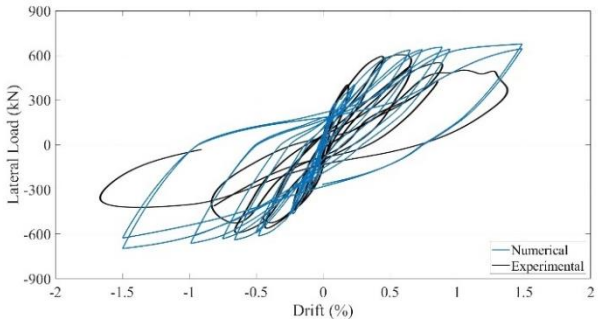

Figure 5. Verification of the numerical analysis

Finite element modeling

A two-dimensional Multiple-Vertical-Line-Element-Model (MVLEM) is created using the MVLEM element approach to simulate the behavior of flexure-dominated RC walls [20-22]. As shown in Figure 1a, a single model element contains six global degrees of freedom, three of which are situated in the middle of the rigid top and bottom beams. A sequence of uniaxial elements (or macro-fibers) attached to the rigid beams at the top and bottom (e.g., floor) levels replicate the axial/flexural response of the MVLEM, while a shear spring positioned at a height *ch* from the bottom of the wall element describes the shear response (Figure 1a). The model element's flexural and shear responses are independent. The point on the element's central axis at height *ch* is where the wall element's top and bottom faces are rotated in relation to one another (Figure 1b). Rotations and associated transverse displacements are computed based on the wall curvature, determined by the section and material parameters, and correspond to each element's bending moment at height ch (Figure 1b). Vulcano et al. (1988) suggested a value of c=0.4 based on a comparison of the model response and the outcomes of the experiments [20].

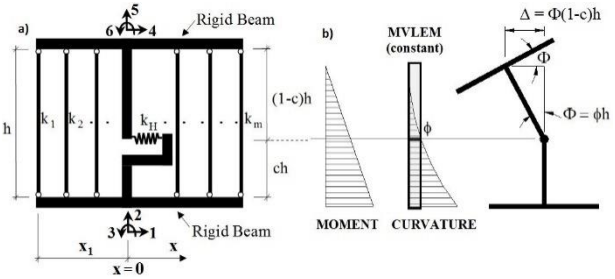

Figure 6. a) MVLEM Element, b) MVLEM Rotations and Displacements [20]

The properties of various SMAs used in this study are shown in "Table 4". These values are directly used in the OpenSees modeling software.

Table 4. Mechanical properties of FeMnAlNi and NiTi [23]

Properties	FeMnAlNi	NiTi
austenite to martensite starting stress (MPa)	320	300
austenite to martensite finishing stress (MPa)	442	450
martensite to austenite starting stress (MPa)	210	200
martensite to austenite finishing stress (MPa)	122	100
superelastic plateau strain length (%)	5	5
modulus of elasticity (GPa)	98	30

Results and discussions

Since the primary goal of this article is to evaluate how equal amounts of memory alloy and steel affect the behavior of the shear wall, the design criteria have not been utilized to replace the steel with memory alloy, and the same quantity of steel has been taken out of the plastic joint on the first story of macro model.

As shown in "Figures 7-9", the use of shape memory alloy in the shear wall will reduce the area under the diagram and, as a result, reduce the dissipated energy of the wall, which is due to the flag-shaped diagram of these alloys and the area under the diagram which is less than the steel rebars alone.

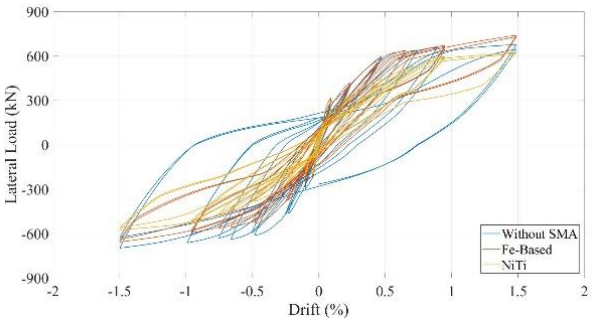

Figure 7. Hysteresis analysis result with SMAs in column

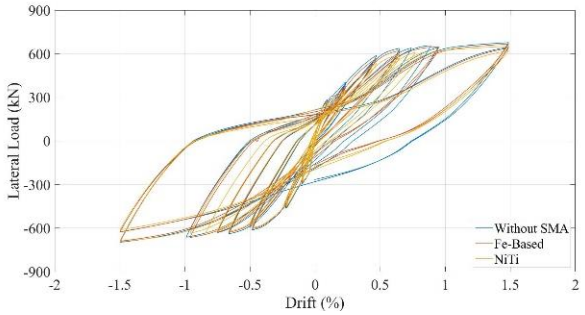

Figure 8. Hysteresis analysis result with SMAs in the middle wall

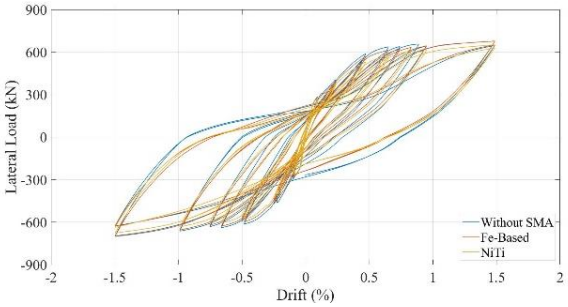

Figure 9. Hysteresis analysis result with SMAs in Beam

The impact of shape memory alloy on residual structural displacement is seen in "Figure 10" and "Figure 11" In all instances where shape memory alloy is utilized in place of steel reinforcement, reduced residual displacement is seen, especially at higher cycles. According to the findings shown in that figure. The least residual displacement is often experienced when shape memory alloy is used in columns in both Fe-based and NiTi SMAs. The use of memory alloy in the middle wall and coupled beam come second in reducing the residual displacement.

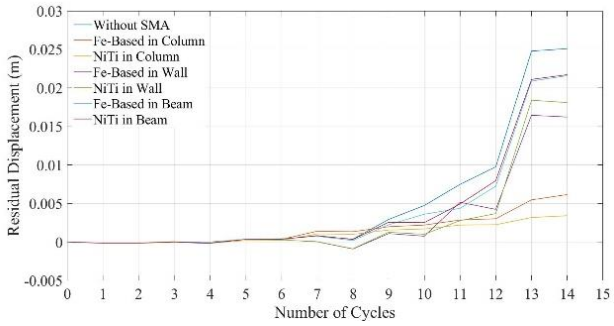

Figure 10. Influence of SMA on residual displacement in positive cycles

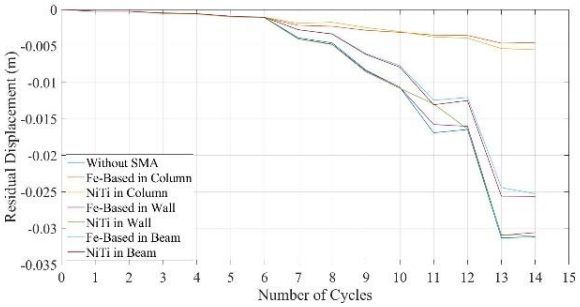

Figure 11. Influence of SMA on residual displacement in negative cycles

Due to their flag-shaped response, it is safe to assume that the reduction in residual displacement strongly correlates to the reduction of dissipated energy from the structural system. The detailed

comparison between the dissipated energy and residual displacement of each type of analysis is presented in "Table 5".

Table 5. influence of SMA on energy dissipation and remained displacement

	Dissipated Energy (kJ)	Maximum negative Residual Displacement (mm)	maximum positive Residual Displacement (mm)
Without SMA	154.34	-31	25
Fe-Based in Wall	131.34	-31	16
NiTi in Wall	123.62	-31	18
Fe-Based in Beam	135.62	-25	22
NiTi in Beam	128.37	-26	22
Fe-Based in Column	74.23	-5	6
NiTi in Column	74.23	-5	3

Additionally, as shown in "figure 12", the structure will experience the highest total dissipated energy if it is exclusively reinforced with steel. Using shape memory alloy in the coupled beam, middle wall, and column will reduce the system's dissipated energy.

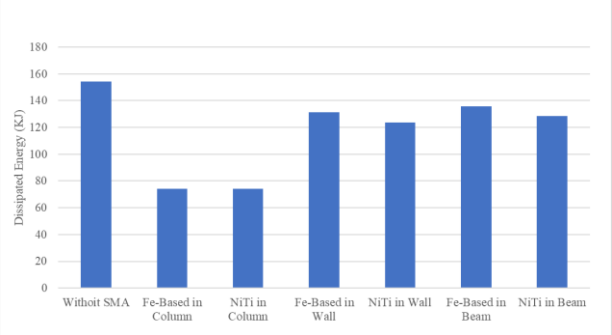

Figure 12. influence of SMA on energy dissipation

Two techniques may describe the best location for replacing steel rebars with SMA. In the first scenario, the ideal location is where the usage of shape memory alloy results in the highest dissipated energy while causing the system to leave the least residual displacement. The second state of optimality is also related to the rate of SMA utilization. The place where the least amount of SMA usage causes the lowest residual displacement. A dimensionless number is used for each of the above states. This dimensionless number for the first scenario is obtained by dividing the percentage of reduction in the residual displacement of the last cycle by the percentage of reduction in the total dissipated energy compared. The larger this dimensionless number is the more appropriate location for using shape memory alloys instead of steel reinforcement. For the second scenario of optimality, the dimensionless number is obtained by dividing the percentage of residual displacement reduction by the percentage of shape memory alloy utilization in the shear wall. In this case, the larger the dimensionless number, the place of replacement is more appropriate.

In "Table 6", the first state of optimality, i.e., optimality of residual displacement-dissipated energy, has been investigated and reported in the 5th column. According to this table, using the memory alloy in the column, in terms of the optimality of the first scenario, is the most optimal place among the available options for using the SMA in shear walls. The second stage of optimization, optimum consumption, is also examined in the 6th column. From the optimality point of view in the second scenario, the ratio with the least residual displacement to the least usage of SMA is the most optimal place among the available replacement regions in the shear wall. Thus, the coupled beam is the best place on average, but it is apparent that the exact best location depends on the type of SMA used.

The residual displacement and dissipated energy reduction in "Table 6" are obtained from comparing SMA reinforced cases with the steel model's results. "Table 7" show the initial stiffness and ultimate strength for different types of SMA as a replacement form of steel reinforcement. This table indicates that due to the different dynamic properties of SMAs, discussed previously in "Table 4", the initial stiffness and ultimate strength of Nitinol are lower than its Fe-based counterpart.

Table 6. Evaluation of two optimization scenarios

	Percentage of utilized SMA	Percentage of residual displacement reduction	Percentage of dissipated energy reduction	Residual displacement to dissipated energy ratio	Residual displacement to utilized SMA ratio
Fe-Based in wall	1.3	18.6	14.9	1.25	14.33
NiTi in wall	1.3	14.0	19.9	0.71	10.80
Fe-based in beam	1.2	16.5	12.1	1.36	13.76
NiTi in beam	1.2	15.7	16.8	0.93	13.05
Fe-based in column	7.4	80.5	51.9	1.55	10.88
NiTi in column	7.4	84.4	51.9	1.63	11.41

Table 7. Influence of SMA on initial stiffness and ultimate strength

	initial stiffness (kN/m)	ultimate strength (kN)
Without SMA	179142	677.7
Fe-based in wall	175186	668.2
NiTi in wall	173779	652.7
Fe-based in beam	176391	677.1
NiTi in beam	174570	651.7
Fe-based in column	170536	739.8
NiTi in column	165987	623.8

Conclusions

Steel has a more substantial capacity to dampen energy than shape memory alloys in all cycles, according to the shape memory alloys' flag-shaped strain stress diagram and their smaller area under the diagram compared to the surface under the steel diagram. The most significant reduction in energy damping capabilities will occur in columns made of shape memory alloys. Using these alloys in the wall and coupled beam results in the most considerable reduction in energy damping ability after the columns. The most significant decrease in residual deformation in the shear wall is brought on by applying shape memory alloy in the column elements. Using SMA in the coupled beam and the wall will minimize the deformation roughly equally after the columns.

Different changes in residual deformation and dissipated energy are observed based on the position and the type of SMA material. For instance, When Fe-based SMAs are utilized to their full potential, the wall is where they have the most significant impact on reducing residual deformation while using the least amount of material. However, different forms of SMA do not compare similarly. It is impossible to pinpoint the exact ideal region for decreasing residual displacement because of SMAs' various behaviors.

In this study, it is observed that the gap between dissipated energy of various SMAs will also close as SMA usage increases.

References

[1] Obata, M., Inoue, M. and Goto, Y., 1998. The failure mechanism and the pull-out strength of a bond-type anchor near a free edge. *Mechanics of materials*, *28*(1-4), pp.113-122.

[2] Fujita, H., Saito, N. and Suzuki, T., 2001. *Operator theory and numerical methods*. Elsevier.

[3] Palermo, D. and Vecchio, F.J., 2007. Simulation of cyclically loaded concrete structures based on the finite-element method. *Journal of Structural Engineering*, *133*(5), pp.728-738.

[4] Ghassemieh, M., Rezapour, M. and Sadeghi, V., 2017. Effectiveness of the shape memory alloy reinforcement in concrete coupled shear walls. *Journal of Intelligent Material Systems and Structures*, *28*(5), pp.640-652.

[5] Dolce, M. and Cardone, D., 2001. Mechanical behaviour of shape memory alloys for seismic applications 1. Martensite and austenite NiTi bars subjected to torsion. *International Journal of Mechanical Sciences*, *43*(11), pp.2631-2656.

[6] Dolce, M. and Cardone, D., 2001. Mechanical behaviour of shape memory alloys for seismic applications 2. Austenite NiTi wires subjected to tension. *International journal of mechanical sciences*, *43*(11), pp.2657-2677.

[7] Shahverdi, M., Michels, J., Czaderski, C. and Motavalli, M., 2018. Iron-based shape memory alloy strips for strengthening RC members: Material behavior and characterization. *Construction and Building Materials*, *173*, pp.586-599.

[8] Bansiddhi, A., Sargeant, T.D., Stupp, S.I. and Dunand, D.C., 2008. Porous NiTi for bone implants: a review. *Acta biomaterialia*, *4*(4), pp.773-782.

[9] Morgan, N.B., 2004. Medical shape memory alloy applications—the market and its

products. *Materials Science and Engineering: A*, *378*(1-2), pp.16-23.

[10] Kang, I., Heung, Y.Y., Kim, J.H., Lee, J.W., Gollapudi, R., Subramaniam, S., Narasimhadevara, S., Hurd, D., Kirikera, G.R., Shanov, V. and Schulz, M.J., 2006. Introduction to carbon nanotube and nanofiber smart materials. *Composites Part B: Engineering*, *37*(6), pp.382-394.

[11] Hartl, D.J. and Lagoudas, D.C., 2007. Aerospace applications of shape memory alloys. *Proceedings of the Institution of Mechanical Engineers, Part G: Journal of Aerospace Engineering*, *221*(4), pp.535-552.

[12] Hartl, M., Giri, A.P., Kaur, H. and Baldwin, I.T., 2010. Serine protease inhibitors specifically defend Solanum nigrum against generalist herbivores but do not influence plant growth and development. *The Plant Cell*, *22*(12), pp.4158-4175.

[13] Bellini, A., Colli, M. and Dragoni, E., 2009. Mechatronic design of a shape memory alloy actuator for automotive tumble flaps: a case study. *ieee transactions on industrial electronics*, *56*(7), pp.2644-2656.

[14] Dolce, M. and Cardone, D., 2001. Mechanical behaviour of shape memory alloys for seismic applications 2. Austenite NiTi wires subjected to tension. *International journal of mechanical sciences*, *43*(11), pp.2657-2677.

[15] Czaderski, C., Hahnebach, B. and Motavalli, M., 2006. RC beam with variable stiffness and strength. *Construction and building materials*, *20*(9), pp.824-833.

[16] Ghassemieh, M., Bahaari, M.R., Ghodratian, S.M. and Nojoumi, S.A., 2012. Improvement of concrete shear wall structures by smart materials. *Open Journal of Civil Engineering*, *2*(3), p.87.

[17] Ghassemieh, M., Ghodratian, S.M., Bahaari, M.R. and Nojoomi, S.A., 2013. Seismic enhancement of coupled shear walls using shape memory alloys. *Journal of Civil Engineering and Science*, *2*(2), pp.93-101.

[18] Warashina, M., Kono, S., Sakashita, M. and Tanaka, H., 2008, October. Shear behavior of multi-story RC structural walls with eccentric openings. In *The 14th world conference on earthquake engineering, Beijing, China* (pp. S15-029).

[19] Wang, J.Y., Sakashita, M., Kono, S., Tanaka, H. and Lou, W.J., 2010. Behavior of reinforced concrete structural walls with various opening locations: experiments and macro model. *Journal of Zhejiang University SCIENCE A*, *11*(3), pp.202-211.

[20] Vulcano, A., Bertero, V.V. and Colotti, V., 1988, August. Analytical modeling of RC structural walls. In *Proceedings, 9th world conference on earthquake engineering* (Vol. 6, pp. 41-46).

[21] Orakcal, K., Wallace, J.W. and Conte, J.P., 2004. Flexural modeling of reinforced concrete walls-model attributes. *Structural Journal*, *101*(5), pp.688-698.

[22] Kolozvari, K., Orakcal, K. and Wallace, J.W., 2015. Shear-flexure interaction modeling for reinforced concrete structural walls and columns under reversed cyclic loading. *Pacific Earthquake Engineering Research Center, University of California, Berkeley, PEER Report*, (2015/12).

[23] Omori, T., Ando, K., Okano, M., Xu, X., Tanaka, Y., Ohnuma, I., Kainuma, R. and Ishida, K., 2011. Superelastic effect in polycrystalline ferrous alloys. *Science*, *333*(6038), pp.68-71.